NeuroImage 219 (2020) 117015

Contents lists available at ScienceDirect

NeuroImage

journal homepage: www.elsevier.com/locate/neuroimage

Spectral fingerprints of correct vestibular discrimination of the intensity of body accelerations

M. Ertl [a,b,*], M. Klaus [a], F.W. Mast [a], T. Brandt [c,e], M. Dieterich [b,c,d]

[a] Department of Psychology, University Bern, Switzerland
[b] Department of Neurology, Ludwig-Maximilians-Universität München, Germany
[c] German Center for Vertigo and Balance Disorders-IFBLMU (DSGZ), Ludwig-Maximilians-Universität München, Germany
[d] Munich Cluster for Systems Neurology (SyNergy), Munich, Germany
[e] Hertie Senior Research Professor for Clinical Neuroscience, Ludwig-Maximilians-Universität München, Germany

ARTICLE INFO

Keywords:
Vestibular stimulation
Vestibular perception
Vestibular evoked potentials
Inter trial phase clustering (ITPC)
Inter site phase clustering (ISPC)
Decision-making
Theta oscillations
Sensation perception transition
Cluster-based permutation test

ABSTRACT

Perceptual decision-making is a complex task that requires multiple processing steps performed by spatially distinct brain regions interacting in order to optimize perception and motor response. Most of our knowledge on these processes and interactions were derived from unimodal stimulations of the visual system which identified the lateral intraparietal area and the posterior parietal cortex as critical regions. Unlike the visual system, the vestibular system has no primary cortical areas and it is associated with separate multisensory areas within the temporo-parietal cortex with the parieto-insular vestibular cortex, PIVC, being the core region. The aim of the presented experiment was to investigate the transition from sensation to perception and to reveal the main structures of the cortical vestibular system involved in perceptual decision-making. Therefore, an EEG analysis was performed in 35 healthy subjects during linear whole-body accelerations of different intensities on a motor-driven motion platform (hexapod). We used a discrimination task in order to judge the intensity of the accelerations. Furthermore, we manipulated the expectation of the upcoming stimulus by indicating the probability (25%, 50%, 75%, 100%) of the motion direction. The analysis of the vestibular evoked potentials (VestEPs) showed that the decision-making process leads to a second positive peak (P2b) which was not observed in previous task-free experiments. The comparison of the estimated neural generators of the P2a and P2b components showed significant activity differences in the anterior cingulus, the parahippocampal and the middle temporal gyri. Taking into account the time courses of the P2 components, the physical properties of the stimuli, and the responses given by the subjects we conclude that the P2b likely reflects the transition from the processing of sensory information to perceptual evaluation. Analyzing the decision-uncertainty reported by the subjects, a persistent divergence of the time courses starting at 188 ms after the acceleration was found at electrode Pz. This finding demonstrated that meta-cognition by means of confidence estimation starts in parallel with the decision-making process itself. Further analyses in the time-frequency domain revealed that a correct classification of acceleration intensities correlated with an inter-trial phase clustering at electrode Cz and an inter-site phase clustering of theta oscillations over frontal, central, and parietal cortical areas. The sites where the phase clustering was observed corresponded to core decision-making brain areas known from neuroimaging studies in the visual domain.

1. Introduction

The correct classification of stimuli is a non-trivial task that consists of multiple processing steps including the encoding of relevant sensory information, evidence accumulation, and drawing a conclusion that is then relayed to the motor output (Pleger and Villringer, 2013). To perform this sensorimotor task, multisensory convergence and interaction between multiple brain areas or networks dealing with different aspects of the classification process is mandatory (Hernández et al., 2010; Hirvonen et al., 2018). Decision-making was most frequently studied with unimodal stimulation of the visual system. Based on the results obtained from the visual domain, decision making is performed by an interplay between

* Corresponding author. University of Bern, Department of Psychology, Fabrikstrasse 8, CH-3012, Bern, Switzerland.
E-mail address: matthias.ertl@psy.unibe.ch (M. Ertl).

https://doi.org/10.1016/j.neuroimage.2020.117015
Received 30 August 2019; Received in revised form 4 May 2020; Accepted 2 June 2020
Available online 4 June 2020

the primary visual cortex and a set of parietal (Huk et al., 2017; Kiani and Shadlen, 2009) and prefrontal brain regions (Hebart et al., 2016; Pisauro et al., 2017).

Cognitive processing of vestibular stimulation is substantially different from visual stimulation in several aspects: First, natural stimulation by body accelerations does not lead to unimodal but rather multimodal stimulation particularly of the vestibular, visual, and somatosensory systems (Ertl and Boegle, 2019). Second, there is evidence that contrary to the existence of a primary visual cortex there is no primary vestibular cortex (Lopez et al., 2012; zu Eulenburg et al., 2012). Early electrophysiological studies in monkeys have shown that vestibular cortical neurons in the posterior insula respond not only to vestibular but also to visual and somatosensory stimuli (Grüsser et al., 1990a, 1990b; Guldin and Grüsser, 1998). Third, the multisensory vestibular system comprises several separate and distinct temporal, parietal, and insular areas with the core area of the parieto-insular vestibular cortex, PIVC, in monkeys (Chen et al., 2011, 2013; Grüsser et al., 1990a) and humans (Brandt et al., 1994; Klaus et al., 2020). Fourth, there is hemispheric lateralization of vestibular function with a preponderance of the right hemisphere in right-handers and of the left hemisphere in left-handers (Dieterich et al., 2003). This lateralization includes the bilateral vestibular system in the upper brainstem and thalamus (Dieterich et al., 2017).

These characteristics of vestibular structures and processing raise the question whether decision-making models as developed for the visual system are similarly applicable for the multisensory vestibular domain. There is a recent psychophysical study which assessed the effect of prior beliefs on the relative probability of motion direction (Ellis et al., 2017). Using a hierarchical drift diffusion analysis, the authors were able to demonstrate that all subjects incorporated the altered prior belief induced by verbal instructions into their perceptual decision-making process. Additionally to the behavioral experiments, a fNIRS study on decision-making during passive motion reported evidence for the involvement of parietal regions in vestibular stimulus discrimination (de Winkel et al., 2017).

In the current study, a vestibular decision-making paradigm was used to test for discrimination of varying intensities of whole-body linear accelerations using a motor-driven motion platform (hexapod). Expectation of body accelerations was modulated by indicating the probability of the next acceleration direction. Temporal and spatial analysis of cortical decision-making processes were performed on EEG data similar to an earlier study on vestibular evoked cortical potentials (VestEPs) with the same platform (Ertl et al., 2017). The key questions of the present study were related to the above described unique structural and functional cortical characteristics of the vestibular system. How does the discrimination task and the modulation via expectation alter early vestibular potentials? Which are the major structures of the cortical vestibular system involved in perceptual decision-making with respect to the involvement of frontal, temporal, and parietal areas and a possible hemispheric lateralization?

2. Methods

2.1. Subjects

Thirty-five healthy subjects (25 female, 10 male) were included in this EEG study. The cohort had a mean age of 26.75 years (SD = 3.75 years). All subjects gave their informed written consent before the experiment and declared that they do not suffer from psychiatric or neurological diseases particularly that they do not have any history of vestibular disorders. All but three subjects declared that they were right-handed. The local ethics committee approved the study. This study was carried out in accordance with the Helsinki Declaration and approved by the local ethics committee of the medical faculty of the Ludwig-Maximilians Universität München, Germany.

2.2. Stimuli

The experiment was conducted on a 6-degree-of-freedom motion platform (Moog© 6DOF2000E) located in the German Center for Dizziness and Balance Disorders (DSGZ), Munich, Germany. For presenting the visual cues a flat screen (JVC GD-463D10: 102 × 57 cm) mounted on the platform about 50 cm in front of the subject was used. The noise produced by the motion platform was masked by presenting white noise via noise-cancelling headphones (Bose QuietComfort 15) during the entire duration of the experiment. The vestibular stimuli consisted of lateral (left/right) translational movements with similar profiles used in previous EEG studies on vestibular processing (Ertl et al., 2017). During the experiment, two stimuli of different maximum acceleration intensities (0.09 g and 0.12 g) were used. Example profiles of a strong and weak acceleration as measured by acceleration sensors ranging from −200 to 800 ms relative to the peak acceleration are provided in the supplementary material (AccSignal.csv) and we included dotted lines showing a weak and strong acceleration in Fig. 2A. The intensities of the stimuli were selected to cause an error in about 25% of the trials. In order to achieve this goal a pilot experiment in which seven subjects performed an acceleration intensity discrimination task with various intensity differences was conducted and the stimuli for the experiment were chosen based on this pilot-data.

2.3. Procedure

During the experiment, the subjects performed 400 trials. Each trial started with an image that contained probabilistic information about the upcoming motion direction displayed for 1.0 s (Fig. 1). The image showed either one or two arrows pointing to the left or to the right. A single arrow indicated the direction of the following movement with 100% certainty. Alternatively, two arrows pointing in opposite directions were presented. In those conditions, the relative size of the arrows contained information on the following movements. The arrows could either be of the same size, which indicated that a movement to the left or right was equally likely, or one of the arrows was significantly bigger than the other. In case of the latter, the probabilities for the subsequent movement were 75%/25% in favor of the bigger arrow. The delay between the offset of the visual cue and the acceleration onset was randomly varied between 1.5 and 2.5 s. A fixation cross appeared after the offset of the visual cue and remained on the screen until 1.5–2.5 s after the motion ended. The fixation cross served to minimize eye-movements. The time between acceleration and deceleration of the motion stimulus was randomized between 630 and 1095 ms (mean = 885 ms; SD = 97 ms). During this interval the platform moved at a constant velocity, before it decelerated with the inverted acceleration profile. Three questions were displayed on the screen after each motion stimulus. At first, the subjects were asked if the experienced acceleration was strong or weak. The second question addressed the certainty regarding the intensity judgment (sure/unsure). The third question was related to the arrows shown before the movement (“Were the arrows indicating the correct direction?”). In the 75% condition responses were counted as correct when the movement corresponded to the 75% arrow. Subjects were explicitly instructed to respond with yes in the 100% and with no in the 50% condition. The third question also served the purpose to control for task compliance and to ensure that the arrows shown prior to each trial were not simply ignored by the subjects.

2.4. Behavioral data analysis

The responses provided by the subjects were extracted from the log-files recorded during the experiment and imported to MATLAB for a detailed analysis. We compared the number of correct answers between the strong and the weak acceleration intensity using a rank-sum test. The rate of correct answers for the three instructions (100%, 75% and 50%)

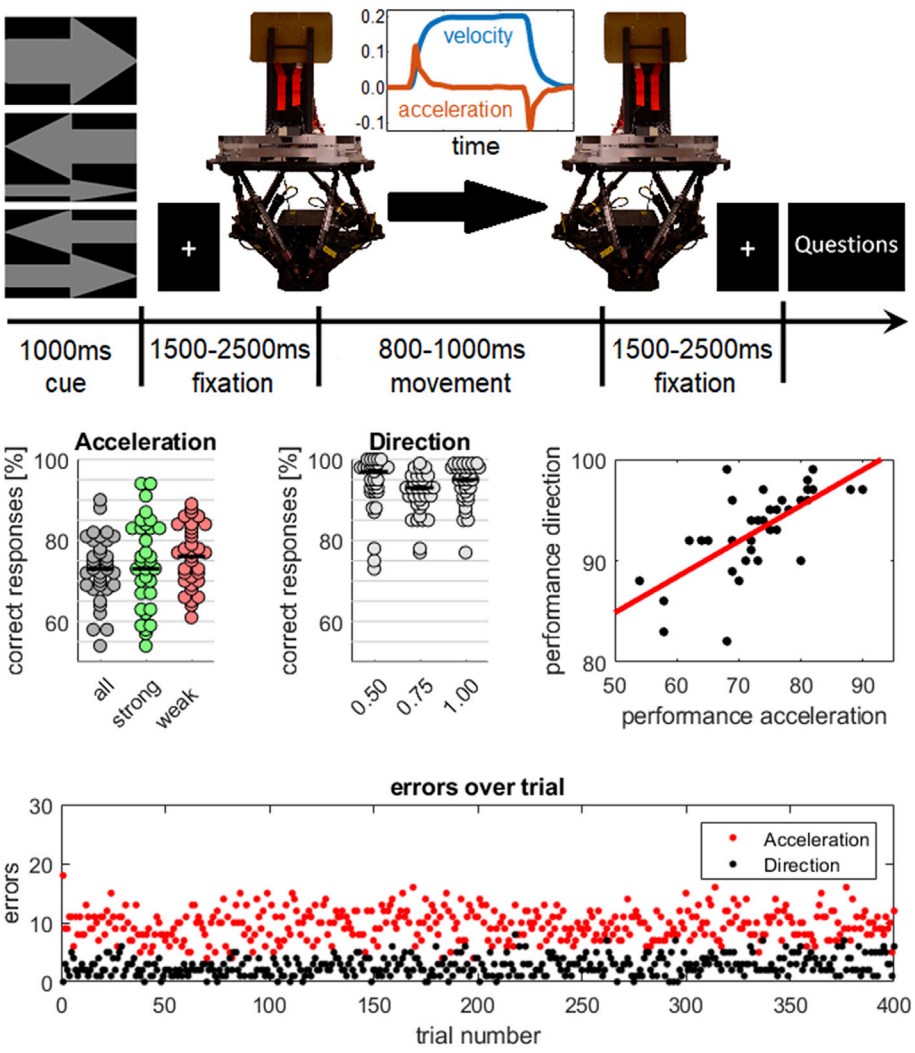

Fig. 1. (Top) Schematic of one trial. Arrows indicating the likelihood of the movement direction (100%, 75%, 50%) were displayed during a 1.5–2.5 s long anticipation phase, followed by a short passive acceleration with a strong or weak acceleration profile. A representative example of the strong acceleration (red) and velocity (blue) profile is displayed. After a rest period the subjects were asked if they experienced a weak or strong acceleration, if they are sure about their classification, and if the movement was in line with the motion direction indicated by the arrows. (Center) Visualization of the main behavioral findings. Center left: Performance of the subjects in correctly classifying the two stimuli as weak or strong. On average (median) the intensity was correctly classified in 73% of all trials. Center middle: Performance of the subjects in reporting the predictive capabilities of the visual cue presented for each platform motion. The average (median) percentage of correct direction responses was 94%. However, the error-rate was significantly higher in the 75% condition compared to the 50% and 100% conditions. Center right: The performance in both tasks was highly correlated. Bottom: Accumulated errors of all subjects over all 400 trials for both tasks. There was no systematic trend, e.g. an increase in error-rate over time or trainings-effects.

were compared using rank-sum tests. In order to test for trainings or fatigue effects we analyzed the errors for the intensity and instruction ratings over time using an ANOVA to compare the error rates for the four blocks of the experiment.

2.5. EEG recording and preprocessing

EEG was recorded using a 32 active EEG channels mounted to standardized elastic caps (actiCaps). The signal obtained by the electrodes was amplified using a BrainAmp MR + Amplifier (Brain Products, Gilching). The signals were recorded by the Brain Vision Recorder in the range from DC – 250 Hz. In addition to the EEG the signals detected by two 3D acceleration sensors were recorded via a Brain Amp ExGr Amplifier. Impedances during the recording were kept below 5kOhm.

The preprocessing was performed using the eeglab toolbox (Delorme and Makeig, 2004) an extension to the MATLAB (Mathworks) Software package. At first data were filtered between 0.01 and 100 Hz using digital filters. All datasets were down sampled to a sampling-rate of 250 samples per second. The reference site was recalculated as the averaged signal across all electrodes. The continuous time traces were epoched from −1500 to 800 relative to the maximum acceleration and an independent component analysis (ICA; infomax) was applied. The calculated components were visually inspected and components clearly reflecting eye- or muscle artifacts (Jung et al., 2000) were removed from the data (average 1.47 components per subjects).

2.6. ERP analyses

We performed multiple event related potential (ERP) analyses on different time windows of the dataset. For every ERP analysis, all relevant segments were inspected for artifacts by means of an automated amplitude based algorithms and segments with values larger than + - 150 μV have been excluded for the particular analysis.

2.7. Statistics

Amplitudes and Power-values derived from EEG data were tested for normality using a Lilliefors-test as implemented in MATLAB. The tests rejected the null-hypothesis that the data come from a distribution in the normal family at a 5% significance level. Therefore, we used non-parametric tests for statistical analyses.

2.8. Vestibular evoked potentials (VestEPs)

In order to investigate the evoked potentials elicited by the acceleration of the motion platform we segmented the data from −200 to 800 ms relative to the maximum acceleration, performed a baseline correction and averaged the data across trials. Additionally, we sorted the trials into the six categories: (I) strong acceleration, (II) weak acceleration, (III) strong acceleration correct, (IV) strong acceleration incorrect, (V) weak acceleration correct, (VI) weak acceleration incorrect. Trials were

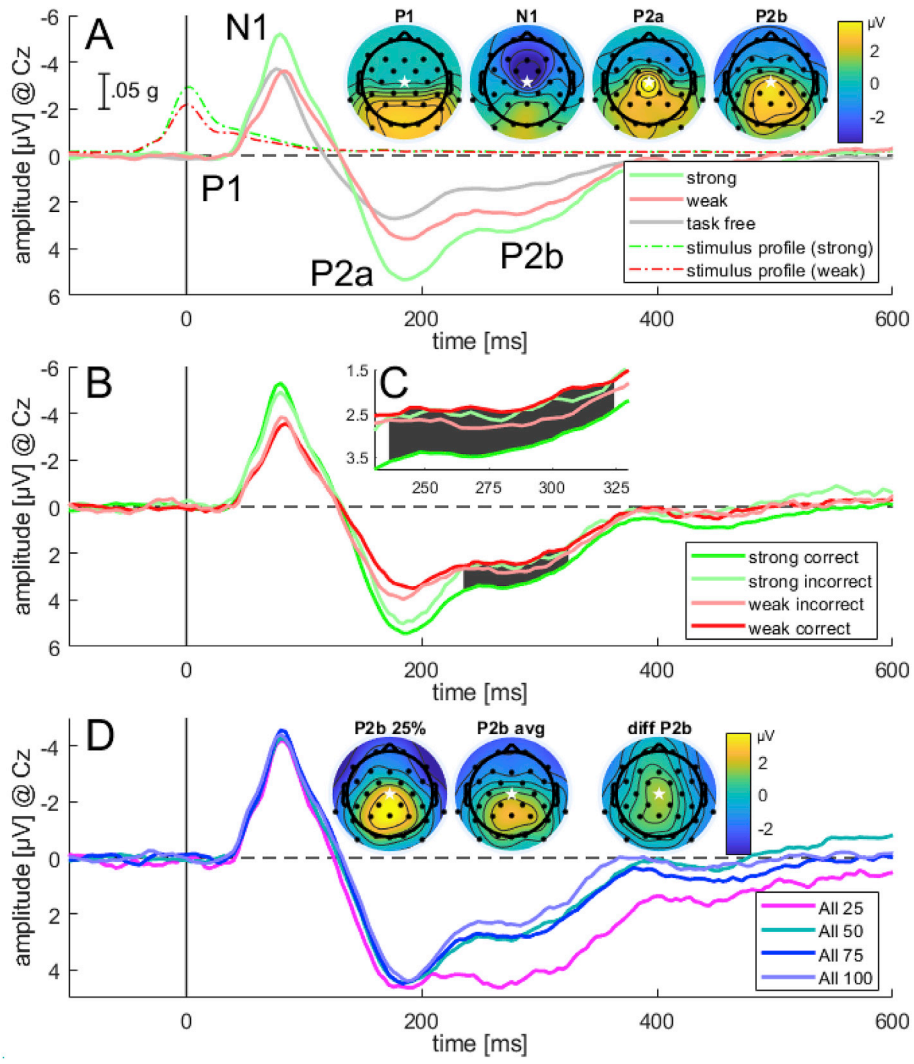

Fig. 2. Visualization of the main results of the ERP analyses. **A:** Grand averages of the time courses for all strong (green) and weak (red) accelerations at electrode Cz (white star). The topographies of the four components P1, N1, P2a, and P2b are displayed. The increase in amplitude with stronger acceleration intensities as well as the topographies nicely replicate previously published findings (Ertl et al., 2017). However, a P2b component was less pronounced in a task-free experiment (grey line). The less focused and more posterior distribution of the P2b compared to the P2a indicates different or additional generators of the component which was confirmed by source estimation (Fig. 5). The dotted lines represent the acceleration profiles as detected by acceleration sensors mounted on the platform. Original data of the acceleration profiles are provided in the supplementary material (AccSignal.csv). **B:** Time courses of the ERPs averaged time course based on the intensities as reported by the subjects. In the beginning, the responses show amplitudes sorted by the physical properties of the stimuli (e.g. acceleration intensity), with the wrongly classified trials showing amplitudes between the correct classified trials and larger amplitudes for strong accelerations. At later times (grey area magnified in **C**), corresponding with the occurrence of the P2b components the order of activity changes and is then in line with the order predicted by detection theory. This might be the transition from sensation to perception **D:** Averages of all trials pooled for both intensities (weak, strong), grouped with respect to the direction-cue and the actual movement. A significantly more pronounced P2b component can be observed in trials where the actual movement was unexpected (25% chance) compared to all other conditions (50%, 75% or 100%). The topographies show the scalp distribution for the P2b in the 25% condition, the average across the other three conditions (P2b avg), and the difference between the two topographies. The occurrence of an unexpected movement resulted in a pronounced positivity at central electrodes.

considered to be correct, if the subjects correctly reported the acceleration intensity performed by the platform in a particular trial and incorrect otherwise. This procedure enabled us to test if the VestEPs showed larger amplitudes for the strong accelerations compared to weak accelerations as found by previous studies. Furthermore, we aimed addressing the question whether the amplitudes differ between correct and incorrect trials. We focused our analyses on two potentials, the N1 and P2, both extensively described in a previous study (Ertl et al., 2017). The N1 amplitudes were defined as the maximum negative deflection in the time interval from 84 to 156 ms. The P2 is a wider component occurring between 176 and 352 ms post acceleration maximum. The P2 was further split into two sub-components, namely a P2a (176–240 ms) and a P2b (240–352 ms). The amplitudes of the P2a and P2b were analogous to the N1 defined as the maximum positive deflection in the respective time windows. For the comparison of the amplitudes between conditions two-sided Wilcoxon rank sum tests were performed.

In addition to the standard approach, we also performed cluster-based permutation tests on the time windows from 0 to 500 ms post acceleration maximum. By using this method we were able to investigate condition differences in two dimensional data (channels x time) by addressing the multiple comparison problem in a nonparametric framework (Maris, 2012; Maris and Oostenveld, 2007). The individual averages for the strong and weak trials were exported to the FieldTrip toolbox (Oostenveld et al., 2011; http://fieldtriptoolbox.org). The ft_timelockstatistics function was used to compare the conditions utilizing a Monte Carlo (2000 randomizations) approach and cluster-based test statistic. A minimum of three neighboring electrodes at the same time was considered as a significant cluster.

2.9. Source localization (eLORETA)

In order to estimate the most-likely generators of the ERP components we used the exact low-resolution brain electromagnetic tomography algorithm (eLORETA), as developed and implemented by Pascual-Marqui (Pascual-Marqui, 2007, 2002) and freely available through the LORETA-webpage (http://www.uzh.ch/keyinst/loreta.htm). LORETA aims to find a unique solution to an ill-posed problem by introducing reasonable assumptions on the processes causing the scalp distribution.

In this study, the single-trial time courses of each subject were exported to the LORETA software package. The time courses were then averaged and a transformation matrix based on the coordinates of the electrode positions was applied to the averaged time courses. Statistical analyses were performed by comparing the average activity of the ERPs (P1, N1, P2a, P2b) to the average pre-stimulus baseline activity. Furthermore, the activity contrast between the P2a and P2b component and between all sure compared to all unsure trials were calculated.

2.10. Time-frequency-analysis

The time-frequency-analysis by means of a wavelet-analysis was

performed using in-house written scripts based on the approaches recommended by Cohen (2017). In a wavelet analysis a collection of wavelets which are sine waves multiplied with a Gaussian kernel are used to estimate the frequency spectrum of a signal at any given time point. Here complex Morlet wavelets were convolved with the single trial EEG data. The epochs ranged from −800 ms to 800 ms. In order to adjust the spatial and temporal resolution of the used wavelets across the analyzed frequency range the number of cycles was increased (logarithmically spaced) for higher frequencies starting with two cycles at 1 Hz and a maximum of 10 cycles at 40 Hz. The calculated magnitudes of the convolution were squared [real(z(t))^2+i(z(t))^2] and this power values were used for the statistical analyses. For the statistical tests, the power values were baseline corrected by frequency wise subtracting the mean power of the pre-stimulus interval.

2.11. Inter trial phase clustering (ITPC) and inter side phase clustering (ISPC)

ITPC measures the extent to which a distribution of phase angles at each time-frequency-electrode point across trials is non-uniformly distributed in polar space. ISPC is a similar measurement but it quantifies the similarity of the phase values between pairs of channels across trials. Phase values are independent of the amplitude of the EEG signal and provide valuable information on underlying neural processes. In fact phase coherency is a key mechanism in information binding and long-range interregional communication (Fries, 2005, 2015; Plankar et al., 2013; Siegel et al., 2012). ITPC is hereby defined as the length of the average vector from a distribution of unit phase angles at one time–frequency point over trials while ISPC can be mathematically defined as the length of the average vector from a distribution of unit phase angle differences between two electrodes at one time–frequency point over trials (Cohen and Gulbinaite, 2014). According to the definition of both metrics, ITPC and ISPC values range from zero (no phase consistency) to one (perfect phase consistency).

3. Results

3.1. Behavioral data

The error rate in the discrimination task was 26.5% (SD: 8.0%) across all conditions and no significant differences were found between the strong and weak condition (Fig. 1). The third question about the actual movement and the prediction by the arrows has been answered correct in 94% (SD: 4.26%) across all conditions (97% in the 50% condition, 93% in the 75% condition, 95% in the 100% condition). In the 75% conditions the error rate was significantly increased compared to the 100% ($p = 0.019$, hedges $G = 0.52$) and the 50% condition ($p = 0.004$, hedges $G = 0.43$). The percentage of correct responses across both questions was highly correlated ($r = 0.68$, $p < 0.001$). The error rate did not change across the four blocks for the acceleration intensity question ($F = 0.27$; $p = 0.85$) and the arrow-direction question ($F = 0.61$; $p = 0.61$). A two-sided *t*-test revealed no significant differences in the performance between female and male subjects.

3.2. VestEPs

The overall time course of the VestEPs revealed a three phasic waveform (P1, N1, P2) as described in previous studies. However, a comparison of the time course obtained in this experiment with the time course of similar left/right accelerations, as recorded and reported earlier (Ertl et al., 2017) revealed an additional positive but less pronounced peak about 150 ms after the known P2 component (Fig. 2A). Comparing the N1 amplitudes of the strong and weak acceleration trials measured at electrode Cz we found significantly ($p < 0.001$, hedges' $G = 0.70$) increased amplitudes for strong accelerations. A similar increase was observable for the P2a and P2b amplitudes ($p < 0.001$, P2a: hedges' $G = 0.47$, P2b: hedges' $G = 0.39$).

A comparison between movements to the left and right side did not reveal any significant difference between the time courses at electrode Cz. In order to test for lateralization effects, we tested for potential differences at the laterally located electrodes C3 and C4. We found significantly increased N1 ($p = 0.025$, hedges' $G = 0.36$) and P2b ($p = 0.039$, hedges' $G = 0.26$) amplitudes at electrode C3 for motions to the left. Analogously, we found increased amplitudes for the N1 ($p = 0.002$, hedges' $G = 0.48$) and P2b ($p = 0.007$, hedges' $G = 0.29$) components at electrode C4 for rightward motions (suppl. Figure 3).

In a subsequent analysis, the amplitudes of the correct and incorrect trials for the strong and weak accelerations were compared using a Kruskal-Wallis test and post-hoc Wilcoxon rank sum tests. The Kruskal-Wallis test revealed altered amplitudes between the four conditions (strong correct, strong incorrect, weak correct and weak incorrect) for the N1 ($p = 0.008$) but not the P2a ($p = 0.091$) or P2b ($p = 0.216$) component (Fig. 2B). The rank sum tests revealed significantly larger amplitudes for the strong correct trials compared to the weak correct (N1: $p < 0.001$, hedges' $G = 0.76$ P2a: $p < 0.001$, hedges' $G = 0.54$, P2b: $p < 0.001$, hedges' $G = 0.52$) and weak incorrect trials (N1: $p < 0.001$, hedges' $G = 0.57$, P2a: $p < 0.001$, hedges' $G = 0.35$, P2b: $p < 0.045$, hedges' $G = 0.18$). The strong incorrect trials showed increased amplitudes compared to the weak incorrect (N1: $p = 0.003$, hedges' $G = 0.46$, P2a: $p = 0.008$, hedges' $G = 0.27$) and to the weak correct trials (N1: $p < 0.001$, hedges' $G = 0.66$, P2a: $p < 0.001$, hedges' $G = 0.45$, P2b: $p = 0.043$, hedges' $G = 0.20$). Furthermore, the amplitudes of the weak correct trials were reduced compared to the weak incorrect trials (P2a: $p = 0.015$, hedges' $G = 0.19$, P2b: $p = 0.008$, hedges' $G = 0.33$). A comparison of the relative magnitude relation of amplitudes for the P2 components shows that the P2a amplitudes reflect the physical properties of the stimuli, meaning that the stronger accelerations caused larger P2a amplitudes. However, the relative magnitude relation of the amplitudes for the P2b component reflect the perceptual evaluation as reported by the responses (Fig. 2C).

The comparison between the three conditions in which the movement was congruent with the expectation of the subjects (50%, 75%, 100%) with the condition where the movement was unexpected and surprising (25% in the 75% condition) revealed a significantly different time course (Fig. 2D). For these events a prolonged P2 component with a particularly more pronounced P2b component (Kruskal-Wallis test $p = 0.002$) could be observed compared to the other three conditions (25 vs 50: $p < 0.001$, hedges' $G = 0.67$, 25vs75: $p < 0.001$, hedges' $G = 0.60$, 25vs100: $p < 0.001$, hedges' $G = 0.83$).

As confidence-related ERP modulations have been observed over parietal areas (Zizlsperger et al., 2014) we used electrode Pz to compare the time-courses between sure and unsure trials. We found a significant difference between the sure and unsure trials emerging about 300 ms after the acceleration maximum and present until the end of the 800 ms long epoch (Fig. 3). Comparing the mean activity in the interval from 188 ms to 800 ms between the sure and unsure trials a significant difference ($p = 0.008$, hedges $G = 0.23$) could be observed.

Cluster-based permutation tests comparing the strong and weak acceleration conditions revealed 6 significant ($p < 0.05$) clusters over the time windows from 0 ms to 500 ms relative to the maximum acceleration. All clusters contained electrode Cz and largely confirmed the temporal structure assumed during the traditional analysis. A clear distinction between the N1, P2a and P2b component could be found with no significant clusters around 120 ms and 240 ms (Fig. 4). Additionally, another cluster over occipital regions peaking simultaneously with the N1 component at Cz was identified by this analysis.

3.3. Source localization (eLORETA)

The estimation of likely generators for the ERP components revealed that a cortical network including the opercular-insular region and area CSv (Fig. 5A) processes vestibular input. By comparing the statistical

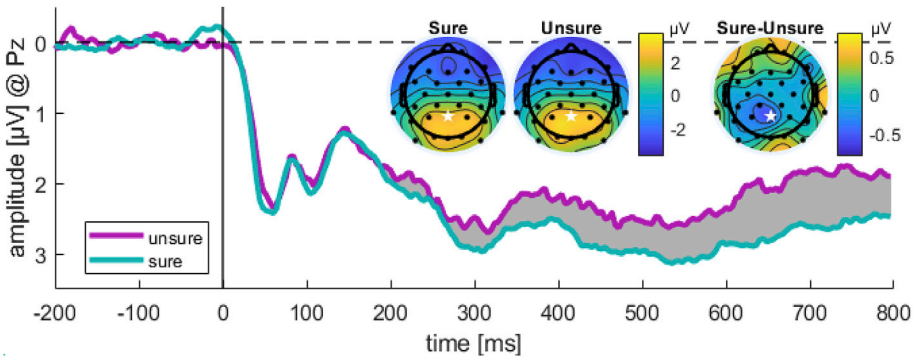

Fig. 3. Average time courses at electrode Pz (white star) of all trials in which subjects reported to be "sure" and "unsure" about their subjective intensity classification. After approximately 190 ms the time-courses diverge and show a more positive deflection when subjects were sure about their classification (grey area). This divergence of the potentials between the conditions shows that meta-cognition, possibly confidence estimation, starts simultaneously with the decision-making process. The topographies visualize the potential distribution for the sure and unsure trials. The difference between the topographies is most pronounced at electrode Pz with a slightly lateralization towards the left parietal electrodes.

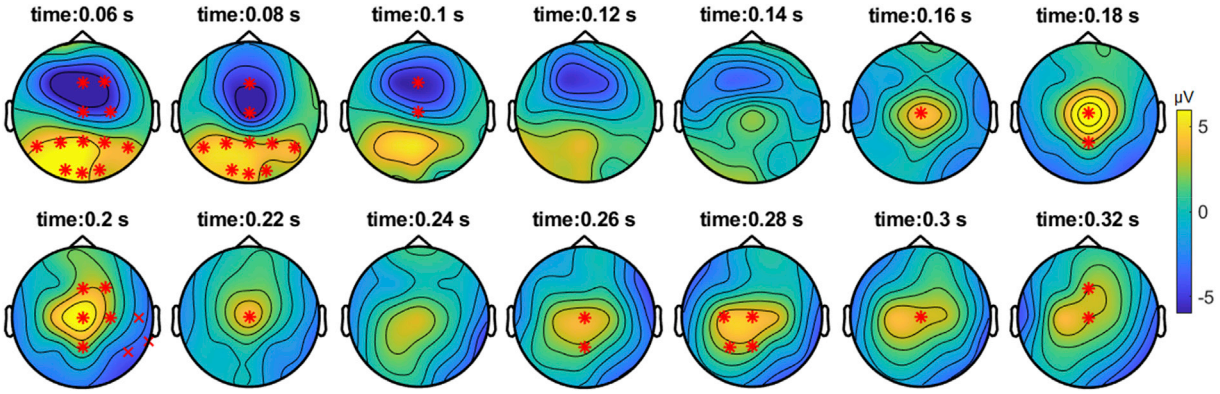

Fig. 4. Results of the cluster-based permutation analysis. The marked electrodes indicate significant differences between the ERPs of the strong compared to the weak condition at the respective time point. All clusters marked with a (*) indicate clusters with a p-value < 0.01, the cluster at 0.2 s, marked with (x) was significant at a p-value < 0.05. The data-driven cluster-based permutation approach confirms the key-role of electrode Cz in vestibular sensation and perception. The analysis also resembles the temporal structure with clusters peaking around 80 ms (N1), 200 ms (P2a), and 280 ms (P2b). Note that at time point 0.06 and 0.08 s two distinct clusters, one occipital and one fronto-central, are present.

maps of the different components we found that - additionally to the known sensory associated areas - the anterior cingulate cortex was a main generator of the N1 and P2a component. The direct comparison of the generators of the P2a and P2b components revealed a significantly ($p < 0.05$) stronger activity in the parahippocampal gyrus, the middle temporal gyrus for the P2b component. However, the anterior cingulate was significantly more active during the P2a interval (Fig. 5B).

The attempt of localizing the difference between the sure and unsure trials observable in the sensor space at electrode Pz did not provided us with an interpretable result, as none of the voxel reached the significance level ($p < 0.05$).

3.4. Time-frequency analysis, ITPC, and ISPC

Analogous to the amplitudes of the VestEP increasing power in the theta-band was observed ($p = 0.038$). The post-hoc tests indicated significantly more 6 Hz power for stronger compared to weaker accelerations and again the incorrectly classified stimuli showed power values between correctly classified weak and strong accelerations. For the strong correct trials the 6 Hz power was significantly increased compared to the strong incorrect ($p = 0.046$, hedges' $G = 0.12$), the weak incorrect ($p < 0.001$, hedges' $G = 0.54$), and the weak correct ($p < 0.001$, hedges' $G = 0.75$) trials. The power of the strong incorrect trials was significantly increased compared to the weak incorrect ($p = 0.001$, hedges' $G = 0.38$) and weak correct ($p < 0.001$, hedges' $G = 0.57$) trials. Additionally, a significant difference was observed comparing the weak correct and weak incorrect trials ($p = 0.018$, hedges' $G = 0.22$).

Comparing the ITPC for 6 Hz oscillations at electrode Cz between all correct (strong and weak) and all incorrect (strong and weak) classified trials in the time interval between 80 and 200 ms we found a significantly increased ITPC ($p < 0.001$, hedges' $G = 1.94$) when trials were correctly classified (Fig. 6).

An investigation of the ISPC for the same frequency and time windows between electrode Cz and all other recording sites revealed significantly (Bonferroni corrected) increased ISPC for correct answers between Cz and Fz ($p < 0.001$, hedges' $G = 0.77$), Cz and P3 ($p < 0.001$, hedges' $G = 0.57$), as well as for Cz and P4 ($p < 0.001$, hedges' $G = 0.57$).

4. Discussion

In the current study, we investigated sensory decision making in a vestibular discrimination task. The experiment was analyzed by performing a standard ERP analysis and investigations in the frequency domain. Three main questions were addressed. Firstly, we were interested in how performing a perceptual discrimination task alters the time course of vestibular evoked potentials (VestEPs) compared to a task-free situation. Secondly, we were interested if and how prior information changes the time course of the VestEPs. Thirdly, we were interested in the question whether we can find traces in ERP patters related to confidence estimations.

Since previous studies showed that theta oscillations play a central role in decision-making processes (Jacobs et al., 2006; Vugt, 2012; Werkle-Bergner et al., 2014; Wokke et al., 2017), we investigated the theta power increase observed at electrode Cz in more detail focusing on phase properties. Interestingly, we found a strongly attenuated ITPC for incorrectly classified trials compared to correctly classified trials regardless of the acceleration intensity (Fig. 6). As inter-site phase relationships have become the center of the popular "communication

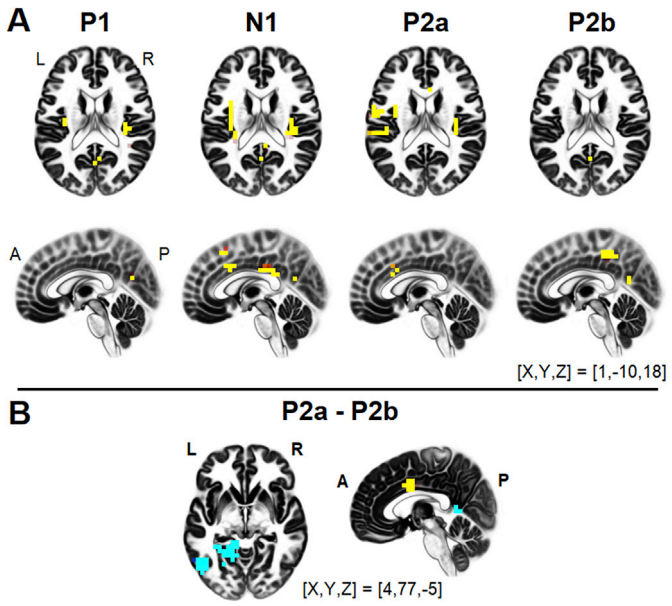

Fig. 5. Visualization of the source localization results. **A:** Main generators of the four identified VestEP components (P1, N1, P2a, P2b) as estimated by eLORETA. The results match the localization results reported in a previous EEG study (Ertl et al., 2017) and also the results of various fMRI and PET studies. The vestibular input is processed by a cortical network including the opercular-insular region (P1, N1, P2a) and area CSv (N1). Additionally, to these areas a contribution of the dorsal anterior cingulate cortex was found for the N1 and P2a but not the P1 and P2b components. **B:** Statistical comparison of the activity in the P2a and P2b time intervals. A significantly ($p < 0.05$) stronger activity in the dorsal anterior cingulate gyrus could be observed for the P2a component (yellow), while during the P2b time window significantly more activity (blue) was generated in the parahippocampal and middle temporal gyri.

through coherence" theory (Fries, 2015; Plankar et al., 2013; Siegel et al., 2012) which aims to explain the mechanisms of inter-regional information exchange in the brain, we further analyzed the phase relations between electrodes. The analysis revealed a significantly increased phase clustering between Cz and three electrodes (Fz, P3, P4) for correctly compared to incorrectly classified trials (Fig. 6). It is possible that the observed signals are spectral fingerprints of large-scale neural interactions of areas involved in the sensory decision-making processes. This conclusion is corroborated by the fact that the positions of electrodes found by the analysis nicely correspond to sites one would expect based on the areas reported by neuroimaging and animal studies. For example it is well known from intracranial animal recordings and imaging studies that neurons in the lateral intraparietal area or the posterior parietal cortex (Huk et al., 2017; Mazurek et al., 2003) as well as frontal regions (Paul et al., 2015) are main areas in sensory decision making. However, further experiments with optimized designs and confirmatory analyses supporting this conclusion are needed.

Comparing the results obtained here with the results of a recent study (Ertl et al., 2017) we could largely replicate the results demonstrating that cortical response of vestibular stimuli consist of three components and that the amplitudes of those are modulated by the stimulus intensities. The earlier components, particularly the N1 component showed, as expected, larger amplitudes for the stronger stimuli. This conclusion was obtained not only by using the standard approach but also by the cluster-based permutation analyses. Both analysis showed comparable results for the strong versus weak acceleration contrast. The cluster-based permutation analysis revealed a further significant difference over occipital electrodes at about the same time as the N1 (80 ms). While this occipital positivity has been described earlier (Ertl et al., 2017), more detailed analyses addressing its role in vestibular processing are needed.

The ERP analysis further showed that incorrectly classified stimuli showed amplitudes between the weak and strong accelerations and the same pattern was observed for theta oscillations (Fig. 6). According to the frame work of detection theory (Ress and Heeger, 2003) one would

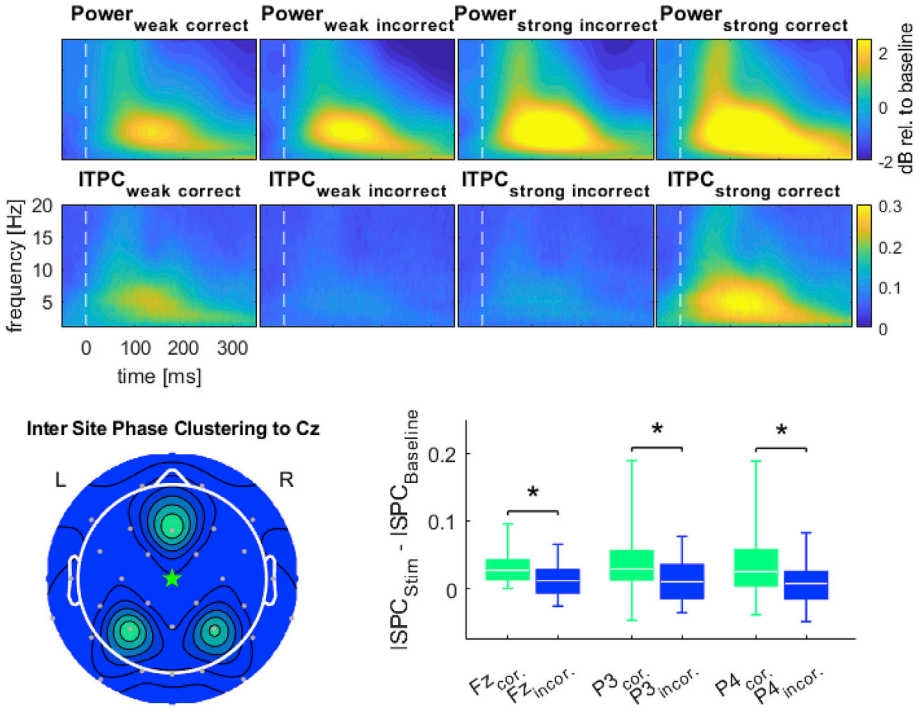

Fig. 6. Top: Comparison of the frequency power between 0 and 20 Hz in the time-interval between −50 and 350 ms for the four conditions (weak correct/weak incorrect/strong incorrect/strong correct. Equivalent to the ERPs a power increase in the theta band can be observed for strong compared to weak trials and the power for misclassified trials is in between the correct trials at electrode Cz. A comparison of the inter trial phase clustering (ITPC) at electrode Cz shows a significantly reduced phase clustering for theta frequencies for incorrect trials compared to the correct trials. Bottom: Analyzing the inter site phase clustering (ISPC) between electrode Cz (green star) and all other 31 electrodes revealed a significantly increased ISPC for the electrode pairs Cz/Fz, Cz/P3, and Cz/P4 for correct compared to incorrect trials in the time interval from 40 to 200 ms for 6 Hz oscillations. The boxplot (bottom right) displays the ISPC for the three pairs of electrodes. The displayed values were baseline corrected by subtracting the average ISPC in the pre-stimulus interval from the values in the investigated time interval. The boxes contain the values between the 25th and 75th percentile, the whiskers indicate the min and max values in the sample and the white horizontal lines represent the median. The increased ITPC in correct trials in combination with the increased ISPC indicates the existence of an interaction between frontal (Fz), central (Cz) and parietal (P3, P4) regions. This interaction seems to be crucial for the correct classification of stimulus properties such as intensities.

expect the miss trials (incorrect strong) to show smaller amplitudes than the false alarms (incorrect weak) and therefore the activity should correlate with the percept and not necessarily with the physical properties of the stimuli (Britten et al., 1996; Nienborg and Cumming, 2006). Our data show such an activity ranking (Fig. 2B, grey area), however not significant, for later time points (>220 ms). This is in line with the established concept that potentials with latencies smaller than 250 ms typically correlate with the physical properties of a stimulus while cognitive processes determine the features of later potentials (Banaschewski and Brandeis, 2007; Brandeis and Lehmann, 1986; Joos et al., 2014). We interpret the reordering of the potentials in the time interval (>220 ms) as the transition from the processing of sensory information to a higher-level perceptual analysis.

A similar idea has been proposed as an interplay between bottom-up and top-down processes at a comparable time window for the auditory domain (Joos et al., 2014). Interestingly, the resorting of the positivity of the four conditions happens at the same time during which the P2b is observable. The P2b component is a second positive, less pronounced peak with a longer latency than the originally described P2 component. The P2b was not observed in a task-free passive acceleration perception experiment (Ertl et al., 2017) and seems to reflect additional cognitive effort. As both components show different scalp distributions (Fig. 2A) with the peak positivity at electrode Pz for the P2b rather than at electrode Cz as for the P2a we assume that the components reflect different processing steps. The direct comparison of the generators of both components showed that the P2a has a significantly stronger contribution of the dorsal anterior cingulate cortex (Fig. 5) which also explains why the strongest positivity is observed more anterior compared to the P2b component on a scalp level. We speculate that overall the P2 complex could represent a neural correlate of the transition from the processing of sensory information to an integrated and interpreted perception.

This idea is supported by the comparison of the P2b amplitudes in the context of the direction cue induced expectations. The time-courses of the four conditions diverge about 200 ms after the maximum acceleration with the P2b most pronounced for the unexpected condition and less distinct for the other three conditions. The significant contribution of the dorsal anterior cingulate cortex during the N1 and P2a time window can be linked to decision making processes (Bush et al., 2002). In fact, a brain region close to the one reported here was found in an auditory choice reaction paradigm while simultaneous EEG-fMRI was recorded (Mulert et al., 2008). By performing an EEG informed fMRI analysis of the auditory N1 component the anterior cingulate cortex was the only area showing an increased activity comparing a high effort to a control condition. This indicates that the anterior cingulate cortex is involved in effortful decision making at early temporal stages.

Based on results of a recently published EEG study on cortical representations of confidence during a visual perception task (Zizlsperger et al., 2014), the ERPs over posterior areas were analyzed. A visual inspection of the ERPs revealed diverging time-courses between "sure" and "unsure" trials at about 188 ms after the acceleration maximum (Fig. 3). From that time point until the end of the analyzed segment (800 ms) the ERP observed in "sure" trials showed a pronounced positivity compared to the "unsure" trials. This finding supports previous observations (Zizlsperger et al., 2014) that confidence builds up as early as the decision making process itself.

Our experiment differs to some extent from other decision-making studies, as we did not ask the subjects to respond as fast as possible. In fact, we aimed to temporally disentangle the sensory processing and decision-making from the motor-response. This enabled us to separate the different processing steps but hindered us from performing complex behavioral analysis such as feeding EEG features into a drift-diffusion model.

In addition to the results on decision making, we found significant lateralization effects with respect to the movement direction at electrode C3 and C4. Lateralization effects during vestibular processing are well established in the context of handedness (Dieterich et al., 2017, 2003) but - to our knowledge - no data exist pointing towards distinct processing of vestibular input with respect to the movement direction. Given the various stages of signal integration from the left and right vestibular end organs on the brain stem level and the existence of crossing and non-crossing ascending tracts (Kirsch et al., 2016) a vestibular origin of the movement direction depending difference seems unlikely. It has to be noted that naturalistic acceleration profiles on a motion platform, as expected, co-activated extra-vestibular sensory systems (Ertl and Boegle, 2019). During acceleration to the right the chair caused a force mostly on the left side of the body surface, and vice versa for accelerations to the left. With respect to the close proximity of the recording sites (C3, C4) to the somatosensory cortex regions, in particular the trunk, neck and head areas, it is possible that somatosensory input differences acting on the right and left side of the body can account for these lateralization effects. The right side of the body is represented in the left hemisphere, and thus, the registered ERPs showed larger amplitudes. The amplitudes of the N1 and P2 components were significantly increased at electrode C3 for movements to the left and at electrode C4 for movements to the right.

The exploratory nature of our study and the small body of literature on EEG in combination with vestibular stimuli required certain analyses that could not be guided by previous studies. Further studies on independent datasets are therefore needed to verify the findings from this study, for example the time windows used for splitting the P2 into subcomponents, and to rule out the possibility of overfitting.

In summary, we found strong evidence for a crucial role of theta oscillations in the communication between frontal and parietal brain regions in the correct classification of stimuli. Additionally, evidence for the temporal dynamics of the various steps during decision-making was presented and associated with specific ERP components. We could demonstrate that the P2a is linked to physical properties of the stimuli and that the P2b is associated with cognitive aspects of stimulus evaluation, such as expectation and decision making.

CRediT authorship contribution statement

M. Ertl: Methodology, Software, Formal analysis, Investigation, Writing - original draft, Visualization. **M. Klaus:** Methodology, Formal analysis, Investigation, Writing - original draft. **F.W. Mast:** Conceptualization, Writing - review & editing, Project administration, Funding acquisition. **T. Brandt:** Conceptualization, Writing - review & editing, Project administration, Funding acquisition. **M. Dieterich:** Conceptualization, Writing - review & editing, Project administration, Funding acquisition.

Acknowledgement

The work was supported by the BMBF (German Federal Ministry of Education - BMBF 01 EO 1401), the German Foundation for Neurology (Deutsche Stiftung Neurologie), the Hertie-Foundation, and the Swiss National Science Foundation (100014-162480).

Appendix A. Supplementary data

Supplementary data to this article can be found online at https://doi.org/10.1016/j.neuroimage.2020.117015.

References

Banaschewski, T., Brandeis, D., 2007. Annotation: what electrical brain activity tells us about brain function that other techniques cannot tell us – a child psychiatric perspective, 5, pp. 415–435. https://doi.org/10.1111/j.1469-7610.2006.01681.x.

Brandeis, D., Lehmann, D., 1986. Event-related potentials of the brain and cognitive processes: approaches and applications. Neuropsychologia 24, 151–168.

Brandt, T., Dieterich, M., Danek, A., 1994. Vestibular cortex lesions affect the perception of verticality. Ann. Neurol. 35, 403–412. https://doi.org/10.1002/ana.410350406.

Britten, K.H., Newsome, W.T., Shadlen, M.N., Celebrini, S., Movshon, J.A., 1996. A relationship between behavioral choice and the visual responses of neurons in macaque MT. Vis. Neurosci. 87–100.

Bush, G., Vogt, B.A., Holmes, J., Dale, A.M., Greve, D., Jenike, M.A., Rosen, B.R., 2002. Dorsal anterior cingulate cortex: a role in reward-based decision making. Proc. Natl. Acad. Sci. U.S.A. 99, 523–528. https://doi.org/10.1073/pnas.012470999.

Chen, A., DeAngelis, G.C., Angelaki, D.E., 2011. A comparison of vestibular spatiotemporal tuning in macaque parietoinsular vestibular cortex, ventral intraparietal area, and medial superior temporal area. J. Neurosci. 31, 3082–3094. https://doi.org/10.1523/jneurosci.4476-10.2011.

Chen, X., DeAngelis, G.C., Angelaki, D.E., 2013. Diverse spatial reference frames of vestibular signals in parietal cortex. Neuron 80, 1310–1321. https://doi.org/10.1016/j.neuron.2013.09.006.

Cohen, M.X., 2017. Multivariate cross-frequency coupling via generalized eigendecomposition. Elife 6, 1–26. https://doi.org/10.7554/eLife.21792.

Cohen, M.X., Gulbinaite, R., 2014. Five methodological challenges in cognitive electrophysiology. Neuroimage 85, 702–710. https://doi.org/10.1016/j.neuroimage.2013.08.010.

de Winkel, K.N., Nesti, A., Ayaz, H., Bülthoff, H.H., 2017. Neural correlates of decision making on whole body yaw rotation: an fNIRS study. Neurosci. Lett. 654, 56–62. https://doi.org/10.1016/j.neulet.2017.04.053.

Delorme, A., Makeig, S., 2004. EEGLAB: an open source toolbox for analysis of single-trial EEG dynamics including independent component analysis. J. Neurosci. Methods 134, 9–21. https://doi.org/10.1016/j.jneumeth.2003.10.009.

Dieterich, M., Bense, S., Lutz, S., Drzezga, A., Stephan, T., Bartenstein, P., Brandt, T., 2003. Dominance for vestibular cortical function in the non-dominant hemisphere. Cerebr. Cortex 13, 994–1007.

Dieterich, M., Kirsch, V., Brandt, T., 2017. Right-sided dominance of the bilateral vestibular system in the upper brainstem and thalamus. J. Neurol. 264, 55–62. https://doi.org/10.1007/s00415-017-8453-8.

Ellis, A.W., Klaus, M.P., Mast, F.W., 2017. Vestibular cognition: the effect of prior belief on vestibular perceptual decision making. J. Neurol. 264, 74–80. https://doi.org/10.1007/s00415-017-8471-6.

Ertl, M., Boegle, R., 2019. Investigating the vestibular system using modern imaging techniques—a review on the available stimulation and imaging methods. J. Neurosci. Methods 326. https://doi.org/10.1016/j.jneumeth.2019.108363.

Ertl, M., Moser, M., Boegle, R., Conrad, J., zu Eulenburg, P., Dieterich, M., 2017. The cortical spatiotemporal correlate of otolith stimulation: vestibular evoked potentials by body translations. Neuroimage 155, 50–59. https://doi.org/10.1016/j.neuroimage.2017.02.044.

Fries, 2005. A mechanism for cognitive dynamics: neuronal communication through neuronal coherence. Trends Cognit. Sci. 9, 474–480. https://doi.org/10.1016/j.tics.2005.08.011.

Fries, P., 2015. Rhythms for cognition: communication through coherence. Neuron 88, 220–235. https://doi.org/10.1016/j.neuron.2015.09.034.

Grüsser, O.J., Pause, M., Schreiter, U., 1990a. Localization and responses of neurones in the parieto-insular vestibular cortex of awake monkeys (Macaca fascicularis). J. Physiol. 430, 537–557. https://doi.org/10.1113/jphysiol.1990.sp018306.

Grüsser, O.J., Pause, M., Schreiter, U., 1990b. Vestibular neurones in the parieto-insular cortex of monkeys (Macaca fascicularis): visual and neck receptor responses. J. Physiol. 430, 559–583. https://doi.org/10.1113/jphysiol.1990.sp018307.

Guldin, W.O., Grüsser, O.-J., 1998. Is there a vestibular cortex? Trends Neurosci. 21, 254–259.

Hebart, M.N., Schriever, Y., Donner, T.H., Haynes, J.D., 2016. The relationship between perceptual decision variables and confidence in the human brain. Cerebr. Cortex 26, 118–130. https://doi.org/10.1093/cercor/bhu181.

Hernández, A., Nácher, V., Luna, R., Zainos, A., Lemus, L., Alvarez, M., Vázquez, Y., Camarillo, L., Romo, R., 2010. Decoding a perceptual decision process across cortex. Neuron 66, 300–314. https://doi.org/10.1016/j.neuron.2010.03.031.

Hirvonen, J., Monto, S., Wang, S.H., Palva, M.J., Palva, S., 2018. Dynamic large-scale network synchronization from perception to action. Netw. Neurosci. 2, 285–302. https://doi.org/10.1162/netn.

Huk, A.C., Katz, L.N., Yates, J.L., 2017. The role of the lateral intraparietal area in (the study of) decision making. Annu. Rev. Neurosci. 40, 349–372. https://doi.org/10.1146/annurev-neuro-072116-031508.

Jacobs, J., Hwang, G., Curran, T., Kahana, M.J., 2006. EEG oscillations and recognition memory: theta correlates of memory retrieval and decision making. Neuroimage 32, 978–987. https://doi.org/10.1016/j.neuroimage.2006.02.018.

Joos, K., Gilles, A., Van de Heyning, P., De Ridder, D., Vanneste, S., 2014. From sensation to percept: the neural signature of auditory event-related potentials. Neurosci. Biobehav. Rev. 42, 148–156. https://doi.org/10.1016/j.neubiorev.2014.02.009.

Jung, T., Makeig, S., Humphries, C., Lee, T., McKeown, M.J., Iragui, I., Sejnowski, T.J., 2000. Removing Electroencephalographic artifacts by blind source separation. Psychophysiology 37, 163–178. https://doi.org/10.1111/1469-8986.3720163.

Kiani, R., Shadlen, M.N., 2009. Representation of confidence associated with a decision by neurons in the parietal cortex. Science 324, 759–764. https://doi.org/10.1007/s10955-011-0269-9.

Kirsch, V., Keeser, D., Hergenroeder, T., Erat, O., Brandt, T., Dieterich, M., 2016. Structural and functional connectivity mapping of the vestibular circuitry from human brainstem to cortex. Brain Struct. Funct. 1291–1308. https://doi.org/10.1007/s00429-014-0971-x.

Klaus, M.P., Wyssen, G.C., Frank, S.M., Malloni, W.M., Greenlee, M.W., Mast, F.W., 2020. Vestibular stimulation modulates neural correlates of own-body mental imagery. J. Cognit. Neurosci. 32, 484–496. https://doi.org/10.1162/jocn_a_01496.

Lopez, C., Blanke, O., Mast, F.W., 2012. The human vestibular cortex revealed by coordinate-based activation likelihood estimation meta-analysis. Neuroscience 212, 159–179. https://doi.org/10.1016/j.neuroscience.2012.03.028.

Maris, E., 2012. Statistical testing in electrophysiological studies. Psychophysiology 49, 549–565. https://doi.org/10.1111/j.1469-8986.2011.01320.x.

Maris, E., Oostenveld, R., 2007. Nonparametric statistical testing of EEG- and MEG-data. J. Neurosci. Methods 164, 177–190. https://doi.org/10.1016/j.jneumeth.2007.03.024.

Mazurek, M.E., Roitman, J.D., Ditterich, J., Shadlen, M.N., 2003. A role for neural integrators in perceptual decision making. Cerebr. Cortex 13, 1257–1269. https://doi.org/10.1093/cercor/bhg097.

Mulert, C., Seifert, C., Leicht, G., Kirsch, V., Ertl, M., Karch, S., Moosmann, M., Lutz, J., Möller, H.-J., Hegerl, U., Pogarell, O., Jäger, L., 2008. Single-trial coupling of EEG and fMRI reveals the involvement of early anterior cingulate cortex activation in effortful decision making. Neuroimage 42, 158–168. https://doi.org/10.1016/j.neuroimage.2008.04.236.

Nienborg, H., Cumming, B.G., 2006. Macaque V2 neurons, but not V1 neurons, show choice-related activity. J. Neurosci. 26, 9567–9578. https://doi.org/10.1523/jneurosci.2256-06.2006.

Oostenveld, R., Fries, P., Maris, E., Schoffelen, J.M., 2011. FieldTrip: open source software for advanced analysis of MEG, EEG, and invasive electrophysiological data. Comput. Intell. Neurosci. https://doi.org/10.1155/2011/156869, 2011.

Pascual-Marqui, R.D., 2007. Discrete, 3D distributed, linear imaging methods of electric neuronal activity. Part 1: exact, zero error localization. http://arxiv.org/pdf/0710.3341, 1-16.

Pascual-Marqui, R.D., 2002. Standardized low resolution brain electromagnetic tomography (sLORETA): technical details. Methods Find. Exp. Clin. Pharmacol. 24D, 5–12.

Paul, E.J., Smith, J.D., Valentin, V.V., Turner, B.O., Barbey, A.K., Ashby, F.G., 2015. Neural networks underlying the metacognitive uncertainty response. Cortex 71, 306–322. https://doi.org/10.1016/j.cortex.2015.07.028.

Pisauro, M.A., Fouragnan, E., Retzler, C., Philiastides, M.G., 2017. Neural correlates of evidence accumulation during value-based decisions revealed via simultaneous EEG-fMRI. Nat. Commun. 8, 15808. https://doi.org/10.1038/ncomms15808.

Plankar, M., Brežan, S., Jerman, I., 2013. The principle of coherence in multi-level brain information processing. Prog. Biophys. Mol. Biol. 111, 8–29. https://doi.org/10.1016/j.pbiomolbio.2012.08.006.

Pleger, B., Villringer, A., 2013. The human somatosensory system: from perception to decision making. Prog. Neurobiol. 103, 76–97. https://doi.org/10.1016/j.pneurobio.2012.10.002.

Ress, D., Heeger, D.J., 2003. Neuronal correlates of perception in early visual cortex. Nat. Neurosci. 6, 414–420. https://doi.org/10.1038/nn1024.

Siegel, M., Donner, T.H., Engel, A.K., 2012. Spectral fingerprints of large-scale neuronal interactions. Nat. Rev. Neurosci. 13, 20–25. https://doi.org/10.1038/nrn3137.

Vugt, M.K. Van, 2012. EEG oscillations reveal neural correlates of evidence accumulation. Front. Neurosci. 6, 1–13. https://doi.org/10.3389/fnins.2012.00106.

Werkle-Bergner, M., Grandy, T.H., Chicherio, C., Schmiedek, F., Lövdèn, M., Lindenberger, U., 2014. Coordinated within-trial dynamics of low-frequency neural rhythms controls evidence accumulation. J. Neurosci. 34, 8519–8528. https://doi.org/10.1523/jneurosci.3801-13.2014.

Wokke, M.E., Cleeremans, A., Ridderinkhof, K.R., 2017. Sure I'm sure: prefrontal oscillations support metacognitive monitoring of decision-making. J. Neurosci. 37, 781–789. https://doi.org/10.1523/jneurosci.1612-16.2016.

Zizlsperger, L., Sauvigny, T., Händel, B., Haarmeier, T., 2014. Cortical representations of confidence in a visual perceptual decision. Nat. Commun. 5 https://doi.org/10.1038/ncomms4940.

zu Eulenburg, P., Caspers, S., Roski, C., Eickhoff, S.B., 2012. Meta-analytical definition and functional connectivity of the human vestibular cortex. Neuroimage 60, 162–169. https://doi.org/10.1016/j.neuroimage.2011.12.032.